# Tissue dissociation for single-cell and single-nuclei RNA sequencing for low amounts of input material

**Gordon Wiegleb**
Georg-August-Universitat Gottingen Fakultat fur Biologie und Psychologie
**Susanne Reinhardt**
Technische Universitat Dresden
**Andreas Dahl**
Technische Universitat Dresden
**Nico Posnien** ( nposnie@gwdg.de )
Georg-August-Universitat Gottingen Fakultat fur Biologie und Psychologie https://orcid.org/0000-0003-0700-5595

**Research Article**

**Keywords:** single-cell RNAseq, single-nuclei RNAseq, Drosophila melanogaster, eye-antennal disc

**Posted Date:** May 11th, 2022

**DOI:** https://doi.org/10.21203/rs.3.rs-1623239/v1

# Tissue dissociation for single-cell and single-nuclei RNA sequencing for low amounts of input material

Gordon Wiegleb[1,2], Susanne Reinhardt[3], Andreas Dahl[3], Nico Posnien[1,4] *

[1] University of Goettingen, Department of Developmental Biology, Justus-von-Liebig-Weg 11, 37077 Goettingen, Germany
[2] International Max Planck Research School for Genome Science, Am Fassberg 11, 37077 Goettingen,
Germany
[3] TU Dresden, Center for Molecular and Cellular Bioengineering (CMCB), DRESDEN-*concept* Genome Center, Fetscherstraße 105, 01307 Dresden, Germany
[4] University of Goettingen, Goettingen Center for Molecular Biosciences (GZMB), Justus-von-Liebig-Weg 11, 37077 Goettingen, Germany

*correspondence: nposnie@gwdg.de

GW: gordon.wiegleb@uni-goettingen.de
SR: susanne.reinhardt@tu-dresden.de
AD: andreas.dahl@tu-dresden.de
NP: nposnie@gwdg.de

## Keywords

single-cell RNAseq, single-nuclei RNAseq, *Drosophila melanogaster*, eye-antennal disc

# Abstract

## Background

Recent technological advances opened the opportunity to simultaneously study gene expression for thousands of individual cells on a genome-wide scale. The experimental accessibility of such single-cell RNA sequencing (scRNAseq) approaches already allowed gaining insights into the cell type composition of heterogeneous tissue samples of animal model systems and emerging models alike. A major prerequisite for a successful application of the method is the dissociation of complex tissue into individual cells, which often requires large amounts of input material and harsh mechanical, chemical and temperature conditions. However, the availability of tissue material may be limited for small animals, specific organs, certain developmental stages or if samples need to be acquired from collected specimens. Therefore, we evaluated different dissociation protocols to obtain single-cells from small tissue samples of *Drosophila melanogaster* eye-antennal imaginal discs.

## Results

We show that a combination of mechanical and chemical dissociation resulted in sufficient high-quality cells. As an alternative, we tested protocols for the isolation of single nuclei, which turned out to be highly efficient for fresh and for frozen tissue samples. Eventually, we performed scRNAseq and single-nuclei RNA sequencing (snRNAseq) to show that the best protocols for both methods successfully identified relevant cell types. However, snRNAseq resulted in less artificial gene expression that is caused by rather harsh dissociation conditions needed to obtain single cells for scRNAseq.

## Conclusion

We present two dissociation protocols that allow isolating single cells and single nuclei, respectively, from low input material. Both protocols resulted in extraction of high-quality RNA for subsequent scRNAseq or snRNAseq applications. If tissue availability is limited, we recommend the snRNAseq procedure of fresh or frozen tissue samples as it is perfectly suited to obtain thorough insights into cellular diversity of complex tissue.

# Background

Gene expression is a central molecular process that coordinates various aspects of organismal life, such as behavior [1] and development [2, 3]. Since differences in gene expression are often associated with variation in organismal phenotypes, comparative gene expression studies are powerful approaches to establish testable biological hypotheses [4]. For instance, differences in the expression of the developmental transcription factor genes *pitx1* and *shavenbaby* cause natural variation in armor plate formation in stickleback fish [5] and trichome formation in *Drosophila* [6], respectively. Similarly, natural variation in paternal care behavior in *Peromyscus* mice and density related stress behavior in zebrafish are tightly linked to differences in the expression of genes coding for the hormone vasopressin [7] and the neuropeptide Parathyroid hormone 2 (Pth2) [8], respectively. Advances in sequencing technologies have been facilitating extensive insights into the regulation of gene expression on a genome wide scale [9, 10]. A common observation of such studies is that gene expression strongly depends on the biological context. The spatial and temporal expression of developmental genes, for example, is tightly regulated throughout development resulting in tissue- and even cell type specific expression profiles [11–14]. In the light of this context-dependent gene regulation, it is becoming increasingly relevant to study gene expression on a cellular level.

Nowadays, multiple sequencing technologies are available allowing to quantitatively analyze the messenger RNA content of single cells [15]. Single-cell RNA sequencing (scRNAseq) has been proven powerful to reveal the cell type composition of complex tissues or organs in model organisms, such as the vinegar fly *Drosophila melanogaster* [16, 17], the nematode *Caenorhabditis elegans* [18] and mouse [19]. Also, biological processes, such as development of the optic lobe of the fly brain [20], cell-cell communication in tumors [21] and immunity [22, 23] have been successfully studied. Since the analysis of scRNAseq data does not require prior knowledge of the tissue of interest, this method is exceptionally well-suited to study the cell type composition of emerging model organisms, such as sponges [24], the cnidaria *Nematostella vectensis* [25], *Hydra vulgaris* [26] and *Clytia hemisphaerica* [27], the annelid *Platynereis dumerilii* [28] and the planarian *Schmidtea mediterranea* [29, 30], the ant *Harpegnathos saltator* [31] and multiple vertebrates [32, 33]. Comparative studies have been performed to reveal divergent and conserved aspects of the motor cortex in human, marmoset, and mouse [34] and during early embryonic development in pigs, humans and cynomolgus monkeys [35].

scRNAseq protocols are composed of the following key steps [36, 37]: 1) The tissue of interest

is dissociated, and individual cells are captured either in microwell plates [38] or in micro-droplets [39]. 2) Individual captured cells are lysed in the microwell, or droplet and the released RNA is enriched for polyadenylated RNA (mRNA), and reverse transcribed into complementary DNA (cDNA). 3) Cell and molecule specific barcodes and Illumina sequencing adapters are ligated, and the cDNA is released and amplified by PCR. 4) The amplified libraries are eventually sequenced using next generation sequencing technologies (e.g. Illumina).

While current scRNAseq technologies allow sequencing up to 10,000 cells in one run [40], many more cells are needed as input material. For instance, mechanical stress during dissociation of complex tissue leads to increased cell death [41]. Additionally, harsh dissociation conditions using enzymes, such as Trypsin, contribute to cell damage [42, 43], altered gene expression [43, 44] and RNA degradation [45]. Due to the high cell loss during dissociation current scRNAseq methods are limited if small tissue samples are analyzed because tissue from multiple animals must be collected to obtain sufficient starting material.

Larval imaginal discs of the vinegar fly *Drosophila melanogaster* are such tiny tissues. These flat epithelial sac-like tissues are specified as about 20 embryonic cells and they grow extensively during larval development to up to 30,000 cells [46–48]. During pupae stages, imaginal discs evert and give rise to external adult organs, such as wings, walking legs, genitals and compound eyes [49]. Imaginal discs are excellent models to study fundamental developmental and cellular processes, such as cell proliferation, tissue patterning and morphogenesis [50, 51]. Due to its highly heterogeneous cell type composition, the eye-antennal disc that gives rise to the compound eye, the dorsal ocelli, the antennae, and most of the head capsule [52, 53] is especially interesting for scRNAseq applications. Moreover, recent comparative work on the evolution of compound eye size and head morphology in *Drosophila* species revealed pervasive variation in these adult traits [54–61]. Accordingly, inter- and intraspecific comparisons of eye-antennal disc development have been successful in revealing underlying developmental and molecular mechanisms [58, 59, 62–64]. While gene expression in late eye-antennal disc have been studied at single cell resolution [65, 66], earlier stages are less accessible due to low cell numbers. Therefore, we evaluated different dissociation, tissue preservation and sequencing methods to establish an efficient protocol for single-cell transcriptomics in eye-antennal discs.

We show that a combination of mechanical and chemical dissociation works best to obtained sufficient and representative cells for single-cell RNA sequencing (scRNAseq). However, we observed artificial expression of stress related genes, which was most likely due to rather harsh dissociation and cell-sorting conditions. As an alternative, we tested different protocols to

isolate single nuclei from fresh and frozen tissue and we show that single-nuclei RNA sequencing (snRNAseq) successfully allowed identifying key cell types without the drawback of stress-response. Our work provides an excellent overview of different single cell sequencing approaches when accessibility to tissue samples is limited.

# Results and Discussion

## Tissue dissociation for scRNAseq with low amount of input material

For RNA sequencing of single cells (scRNAseq), heterogenous tissue samples need to be dissociated into live and intact cells. Since about 10,000 cells can be analyzed using the 10x Genomics Chromium System and about 50% of input cells are lost throughout the preparatory steps, we first tested different dissociation protocols to obtain about 20,000 cells from entire larval organs or about 30 eye-antennal imaginal discs at 120 hrs after egg laying (AEL).

The success of different tissue dissociation protocols was evaluated by estimating the ratio of dead and live cells, as well as the final number of live cells. A dead cell staining with Trypan blue is well-established in homogeneous cell suspensions obtained from cell culture [67, 68]. However, we experienced unreliable dead/live cell ratios with our complex cell suspensions, which was most likely due to Trypan blue positive debris. Therefore, we applied a live-dead assay based on propidium iodide (PI) and Calcein green/violet to identify dead and live cells, respectively. This method allows enrichment of live cells via fluorescence activated cell sorting (FACS), which efficiently also removed debris (Supplementary Figure S1A). Note that the combination of PI and Calcein violet resulted in the most efficient separation of live and dead cells due to a lower spectral overlap of both dyes during FACS. Sorted cells were examined by fluorescent microscopy to confirm that they were mostly Calcein positive and PI negative.

First, we tested purely enzymatic or mechanical dissociation protocols, respectively. Incubation of eye-antennal discs in 10x TrypLE and 2.5 mg/ml Collagenase even for 2 hrs did not result in single cell solutions based on visual assessment. Imaginal discs ground with a Dounce homogenizer showed a high proportion of debris and what appeared to be single-nuclei suspensions. Additionally, different attempts resulted in inconsistent dissociation because the low amount of input tissue was barely visible and due to the manual component, it was difficult to balance complete dissociation with the destruction of cells. Based on these observations we reasoned that efficient tissue dissociation required a combination of enzymatic dissociation with gentle mechanical force.

The basic protocol was based on treatment of the tissue with TrypLE and Collagenase on a

shaker at 300 rpm with pipet strokes (1000 µl pipet tips) during and after the incubation. We varied the following parameters (see Supplementary Table S1): enzyme concentration (1x and 10x TrypLE; 2.5 mg/ml and 10 mg/ml Collagenase), incubation time (10 – 60 minutes), incubation temperature (37°C and 30°C), number of pipet strokes (5 strokes during the incubation and 17-20 strokes after the incubation) and filtration of the cell suspension (no filter, 20 µm and 35 µm filters). 1x TrypLE was insufficient to achieve complete dissociation in a timely manner and the addition of 10 mg/ml Collagenase resulted in an increased yield, as well as less cell aggregates (visual assessment). Incubation for up to 60 minutes at 30°C resulted in comparable or slightly more live cells compared to a digestion at 37°C. Filtration with a filter of 35µm mesh size did not drastically reduce the proportion of live cells but decreased the amount of debris. The number of pipet strokes after incubation had the highest impact on cell survival with significantly reduced cell survival after more than 17 strokes. We obtained the best results with 16,208 live cells (58 % survival rate) from 28 eye-antennal discs after 60 minutes incubation at 30°C in 10x TrypLE and 10 mg/ml Collagenase and 5 pipet strokes during and 17 pipet strokes after the incubation (Supplementary Figure S1B). RNA extracted from this sample was of high quality (Supplementary Figure S2) and suitable for 10X Genomics scRNAseq.

In summary, for low amount of input material, such as < 50 late L3 eye-antennal discs we propose a protocol that combines enzymatic dissociation in conjunction with slight mechanical disruption.

## scRNAseq reveals relevant cells and a major impact of heat shock and ribosomal genes

Next, we subjected cells obtained after FACS to a 10X Genomics Chromium run to test if the established dissociation protocol resulted in representative cell types expected in the eye-antennal disc. After droplet-based isolation of RNA from individual cells and subsequent Illumina sequencing, we obtained almost 200 million reads from about 14,500 cells with 13,303 reads and 537 genes per cell (Table 1). 12,000 cells showed less than 10 % mitochondrial gene expression (Figure 1A) confirming that we mostly isolated live cells. Among the top ten genes with most variable expression across cells, we found two heat shock related genes (*Hsp23* and *lncRNA:Hsromega*, Figure 2A) and many reads of the scRNAseq dataset mapped to genes coding for heat shock proteins (Figure 1C), suggesting that the 30°C incubation temperature during dissociation or/and the FACS may impose stress on the cells.

The distribution of reads also showed a high expression of cytoplasmic genes, such as *eEF1alpha1* and eukaryotic elongation factors. Additionally, a lot of genes coding for ribosomal proteins were expressed in our dataset (Figure 1C). The high content of ribosomal genes is expected for scRNAseq because cytoplasmic mRNA is extracted and ribosomal RNAs are known to be very stable [69, 70]. However, they are often considered uninformative.

**Table 1:** Summary statistics for the cell- and nuclei dataset.

| **Dataset** | **Cell** | **Nuclei_MDC** |
|---|---|---|
| ***Estimated Number of Cells*** | 14,487 | 9,048 |
| ***Median Genes per Cell*** | 537 | 812 |
| ***Mean Reads per Cell*** | 13,303 | 13,334 |
| ***Valid Barcodes*** | 96.10% | 97.10% |
| ***No. of Reads*** | 192,731,871 | 120,649,741 |
| ***Fraction of Reads in Cells*** | 38.20% | 73.50% |
| ***Total Genes Detected*** | 11,062 | 12,296 |
| ***Median UMI Counts per Cell*** | 1,249 | 1,383 |
| ***Reads Mapped to Genome*** | 93.20% | 85.70% |
| ***Reads mapped confidently to genome*** | 86.40% | 84.50% |
| ***Reads Mapped Confidently to Intronic Regions*** | 2.10% | 14.70% |
| ***Reads Mapped Confidently to Intergenic Regions*** | 9.00% | 0.80% |
| ***Reads Mapped Confidently to Exonic Regions*** | 75.20% | 69.00% |
| ***Percentage of cells with high mitochondrial read count (>10%)*** | 14.00% | 0.02% |

We performed an unbiased cluster analysis based on variable gene expression to identify major cell types. Among the top four genes that define a certain cluster, we found well-known genes involved in different processes during eye-antennal disc development. For instance, *cut*, which is expressed in antennal tissue of the disc [71, 72] was strongly expressed in cells of clusters 2 and 6, while the retinal gene *twin of eyeless (toy)* [73] was predominantly expressed in cells of clusters 9 and 15 (Figure 2B). The ocelli marker gene *ocelliless/orthodenticle (oc/otd)* [74] could be detected in cells of cluster 18 and *homothorax (hth)*, which is broadly expressed in the eye-antennal disc [71, 75, 76] was found in cells of clusters 2, 6, 7, 17 and 18 (Figure 2B). Clusters 14 and 15 were predominantly defined by expression of members of the enhancer of split gene complex (Figure 2B), which are broadly expressed in the dynamic differentiation wave, the so-called morphogenetic furrow [77, 78]. Overall, we found major eye-antennal disc marker genes for different cell clusters allowing to define meaningful cell types in accordance with previous scRNAseq data obtained for late L3 eye-antennal discs [65]. Gene ontology (GO) term enrichment analyses for marker genes defining each cell cluster (Supplementary Table S2) further confirmed that cells in each cluster expressed genes involved in relevant biological

processes (Supplementary Table S3).

Besides these relevant biological findings, the potential stress response of the cells was also evident in our cluster analysis because three heat shock genes were among the top four cluster defining genes (*Hsp23*, *Hsp26* and *Hsp68*; Figure 2B). Those three genes were expressed in most cells of all clusters, and they showed very high expression in cluster 7 (Figure 2B).

In summary, our tissue dissociation protocol successfully resulted in a cell suspension containing major cell types of the eye-antennal disc but may pose stress on the cells which is detectible through high expression of heat shock genes. Additionally, the high level of ribosomal genes may introduce a bias during further analysis of such data.

## Cryo-preservation of imaginal discs for efficient isolation of single nuclei

Our scRNAseq data suggested that the applied dissociation conditions were still stressful for the cells. Additionally, the protocol relies on the processing of fresh tissue samples hampering the analysis of even smaller tissue samples. For instance, eye-antennal discs at the late L3 larval stage contain about 60,000 cells, while discs at the transition from the L2 to the L3 stage are only composed of about 5,000 cells [79]. Therefore, about 12 times more discs are needed to obtain sufficiently high cell numbers for scRNAseq applying our single cell dissociation protocol. As tissue growth is an integral part of developmental processes, more efficient protocols are needed to harness the full potential of single cell sequencing methods for developmental biology. To this end, we tested two main approaches: First, we evaluated the use of single nuclei for RNA sequencing (i.e. snRNAseq) as snRNAseq has been shown to result in comparable data, especially for tissue samples that are difficult to dissociate into single cells [80–83]. Second, we tested the effect of cryo-preservation on the subsequent isolation of single nuclei and RNA integrity as this step allows collecting small tissue samples over time.

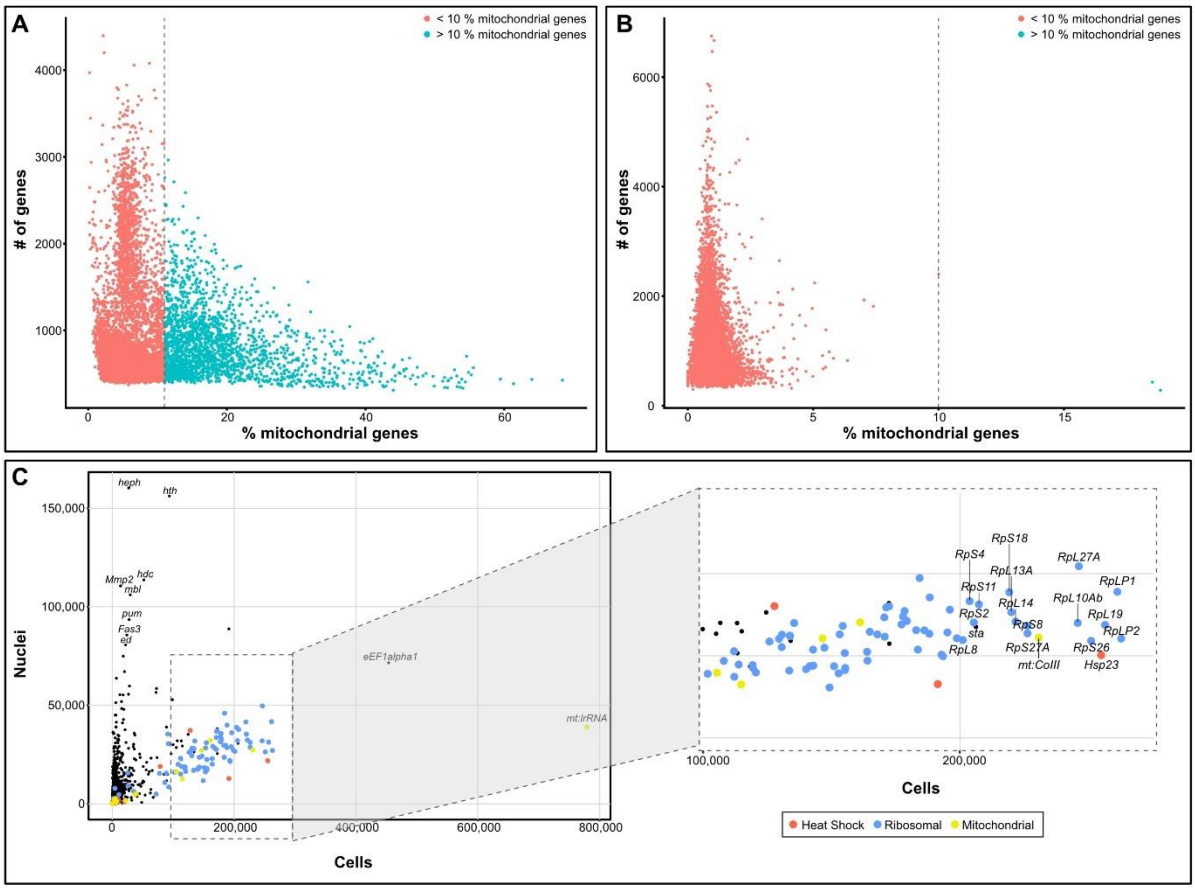


**Figure 1. Evaluation of read distribution after scRNAseq and snRNAseq.**
(**A**) Total amount of genes (features) over percentage of mitochondrial reads, per cell each. The dashed line indicates a threshold of 10% of reads attributed to mitochondrial genes. In single-cell RNA sequencing data, approximately 14% of cells show a high (>10%) proportion of mitochondrial gene reads on the total number of reads. | (**B**) Total amount of genes (features) over Percentage of mitochondrial reads, per cell each in single-nuclei RNA sequencing data. The dashed line indicates a threshold of 10% of reads attributed to mitochondrial genes. In most nuclei, only a low percentage of reads is attributed to mitochondrial genes. | (**C**) Number of reads found in nuclei (y-axis) over the number of reads of those same genes found in cells. The basis are normalized datasets. Ribosomal genes are highlighted in blue and heat shock genes in red. Ribosomal genes are defined as genes starting RpS- or RpL-. Heat shock genes are defined as genes encoding heat shock proteins, starting Hsp-.

For the isolation of single nuclei, we tested two main protocols: One protocol suggested by 10X Genomics is based on NP40 as detergent and a small number of centrifugation and pipetting steps [84]. The other protocol had been established for human heart tissue and is based on using Triton X-100 as a detergent and a variety of RNAse inhibitors to preserve RNA in single nuclei [85]. When 30-50 freshly dissected eye-antennal discs at late L3 stage were used for nuclei isolation, both protocols resulted in more than 20,000 nuclei and extracted RNA was of high quality suitable for snRNAseq (Supplementary Figure S3).

We next dissected imaginal discs, snap-froze them in liquid nitrogen and stored them at -80°C for at least one day, or up to four weeks. All applied protocols allowed us to isolate more than 20,000 intact nuclei from about 30 cryo-preserved eye-antennal discs. RNA extracted from nuclei isolated with the 10X Genomics protocol resulted in low RNA quality, suggesting a high

level of RNA degradation (Supplementary Figure S4, lanes 7 and 8). The addition of Citric acid to the dissociation buffer has been shown to preserve RNA integrity in human pancreatic cells [86]. However, the use of Citric acid during the 10X Genomics protocol did only marginally improve the quality of RNA extracted from cryo-preseved samples (Supplementary Figure S4, lanes 10 and 11). In contrast, we observed almost no RNA degradation and high RNA quality when we used the protocol that employs RNAse inhibitors (Supplementary Figure S4, lanes 1, 2, 4 and 5). RNA integrity was preserved even when eye-antennal discs were thawed for 3.5 hrs and frozen again prior to nuclei isolation and RNA extraction (Supplementary Figure S3), showing that the use of RNAse inhibitors are highly efficient to prevent RNA degradation when processing of cryo-preserved tissue samples. Based on the high yield and the high RNA quality, we conclude that the combination of cryo-preservation and nuclei isolation employing RNAse inhibitors is highly efficient to process low input material for snRNAseq.

## snRNAseq is comparable to scRNA and reduces technical biases

To test if the nuclei obtained after cryo-preservation are suitable for snRNAseq and represent main cell types of the eye-antennal disc, we subjected the nuclei to a 10X Genomics run to obtain 120 million read
s from about 9,000 cells with 13,334 reads and 812 genes per cell (Table 1). For the analysis of the data, we applied the same pipeline and settings as for the scRNAseq dataset, with the exception that intronic reads were included because pre-mRNA is expected in nuclei [83]. Among the 10 genes with most variable expression in the dataset, we found some with known functions and expression in late L3 eye-antennal discs. For instance, the homophilic cell adhesion molecule Klingon (Klg) is strongly expressed during R7 photoreceptor development [87] and *rotund* (*rn*) that codes for a Kruppel zinc-finger transcription factor is expressed in large parts of the antennal field [88]. Importantly, we did not observe genes associated with heat shock response among the top 10 variable genes (Figure 2C) and no bias of reads originating from heat shock genes was observed (Figure 1C), suggesting that they will not impact the subsequent clustering analysis as observed for the scRNAseq data. As expected for snRNAseq data [80, 82, 89, 90], we found only two cells with more than 10 % mitochondrial gene expression (Figure 1B) and much less reads originating from ribosomal genes (Figure 1C). In fact, we observed 28 % less reads of ribosomal genes in the snRNAseq dataset compared to the scRNAseq data, assuming lower impact on the entire dataset.

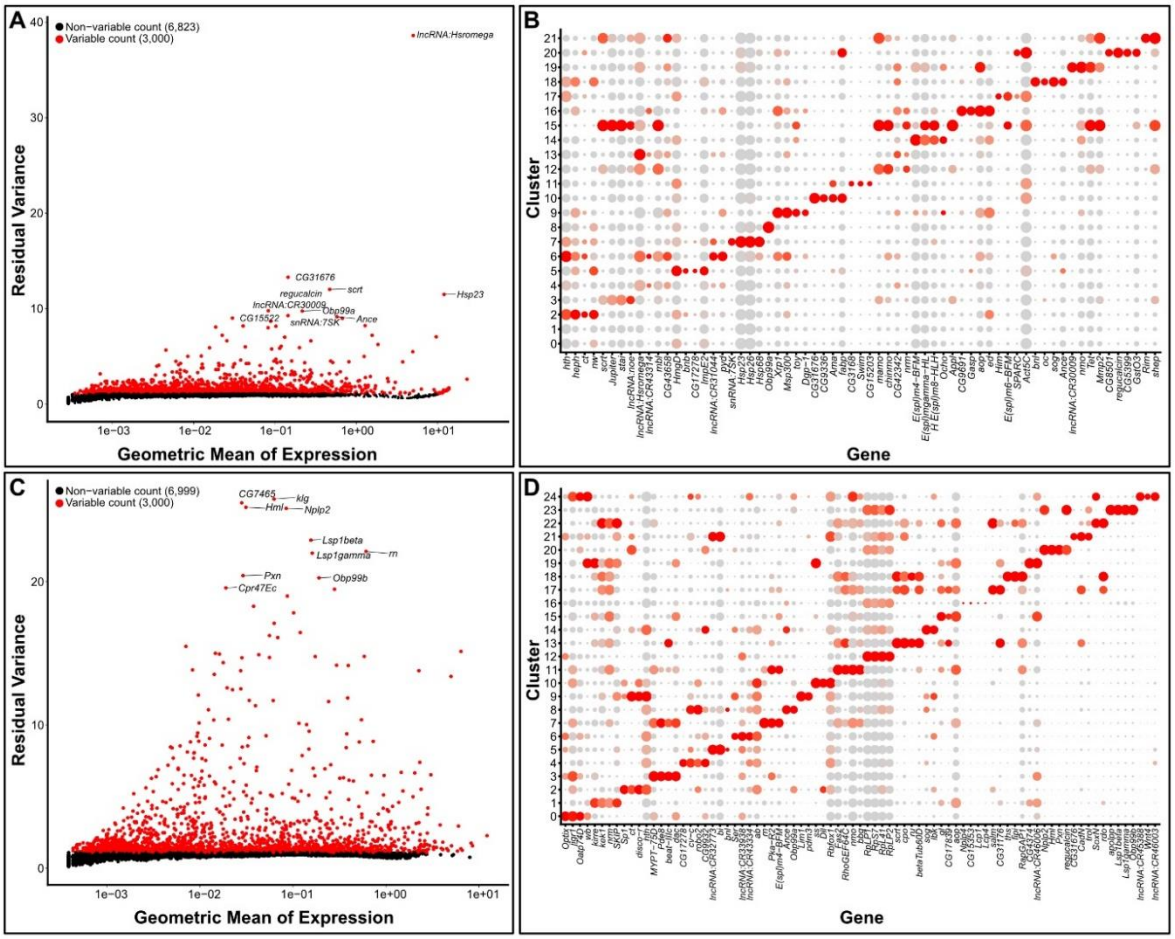


**Figure 2. Most variable genes and marker genes for cell clusters after scRNAseq and snRNAseq.**
**(A)** Variable feature plot of scRNAseq data of dissociated cells. The top 10 variable genes are labeled. These genes are the ones having the strongest influence on clustering and cell type identification. **(B)** Dot plot of the top 4 marker genes (X-axis) for each cell cluster (Y-axis) obtained after scRNAseq. The size of the dots represents the percentage of cells expressing each gene. The color intensity represents the average expression level. **(C)** Variable feature plot of snRNAseq data of isolated nuclei. The top 10 variable genes are labeled. These genes are the ones having the strongest influence on clustering and cell type identification. **(D)** Dot plot of the top 4 marker genes (X-axis) for each cell cluster (Y-axis) obtained after snRNAseq. The size of the dots represents the percentage of cells expressing each gene. The color intensity represents the average expression level.

An unbiased clustering of the snRNAseq data resulted in 24 unique clusters. A closer examination of the top four genes that define a certain cluster we found for instance *Sp1* [91], *cut* (*ct*) [72], *disco-related* (*disco-r*) [92] and *homothorax* (*hth*) [71, 75, 76] in clusters 2 and 9 (Figure 2D). As all four genes are expressed in the antennal region of the eye-antennal disc and have been implicated in antennal development we conclude that these nuclei originated from antennal tissue. Similarly, we observed expression of *Fasciclin 2* (*Fas2*) [93], *nemo* (*nmo*) [94], *big bang* (*bbg*) [95] in cluster 11 (Figure 2D), suggesting that these nuclei contribute to the morphogenetic furrow and differentiating photoreceptors. GO term enrichment analyses for marker genes defining each cell cluster (Supplementary Table S4) revealed biological processes relevant for eye-antennal disc cells (Supplementary Table S5).

We conclude that the snRNAseq dataset captured relevant cell types present in the eye-antennal disc at the late L3 larval stages. At the same time, technical artefacts, such as heat shock gene expression and an excess of reads from ribosomal genes were diminished in snRNAseq.

# Conclusion

Assessing genome wide gene expression for individual cells has proven powerful to describe the heterogeneity of complex tissues, identify novel cell types and to study biological processes, such as immunity and cell-cell interactions at unprecedented detail. Despite the technological advances, single-cell RNA sequencing (scRNAseq) methods still require many cells as starting material. Therefore, we evaluated different dissociation protocols and compared scRNAseq to single-nuclei RNA sequencing (snRNAseq) with special emphasis on low-input material. Based on data obtained for eye-antennal imaginal discs of *Drosophila melanogaster*, we found snRNAseq superior to scRNAseq for the following reasons: 1) The isolation of nuclei requires less experimental steps compared to tissue dissociation into live cells, increasing reproducibility across experiments. This feature is especially relevant if gene expression comparisons are needed on the level of individual cells, for example to assess the effect of experimental manipulations, to study different developmental stages or to compare species/populations. 2) In our evaluation experiment, we observed significantly reduced stress-related expression responses and reduced ribosomal gene expression in snRNAseq data, suggesting that more informative reads contribute to biological insights. 3) We showed highly efficient nuclei isolation and high-quality RNA extraction from frozen tissue [see also e.g. 96]. It is a major advantage to have the opportunity to collect tissue over time and process samples simultaneously, especially for low-input material. 4) In line with previous reports [80, 82, 83, 89, 90, 97–99], our snRNAseq dataset contained sufficient expression information to unravel major cell types expected in eye-antennal imaginal discs. 5) While scRNAseq has been shown to result in biased cell composition, due to different cell sizes, shapes, and survival rate upon dissociation [100], the more streamlined nuclei isolation procedure ensures a more representative assessment for snRNAseq, especially for complex organs, such as nervous tissue including glia cells [81].

It is important to consider major differences in the analysis and interpretation of scRNAseq and snRNAseq data. For instance, snRNAseq data contains intronic reads originating from immature nuclear RNA [83]. Accordingly, well-annotated genome resources are advantageous

and analyses pipelines need to be adjusted to also include reads mapped to introns in subsequent read quantification. snRNAseq data captures only rather transient nuclear RNA, while scRNAseq also includes cytoplasmic mature mRNA. Hence, gene regulation events acting on the level of nuclear export [101, 102], splicing [103] or mRNA maturation [104, 105] may contribute to differences in expression information derived from nuclei and cells, respectively. If cytoplasmic RNA molecules are of special interest and thus single cells need to be isolated, we strongly suggest a dissociation protocol combining chemical and mechanical treatment of tissue samples in conjunction with FACS-aided life cell selection based on fluorescent life-dead cell staining.

In summary, based on a thorough evaluation of different dissociation and sequencing protocols we suggest a highly efficient snRNAseq procedure to obtain high-quality expression data for individual cells. Our procedure is specifically tested for low-input material and will therefore be perfectly suited for future studies with limited access to tissue samples.

# Methods

## Fly stock keeping and tissue dissection

Flies of the Oregon R strain of *Drosophila melanogaster* were kept in fly food vials (400 g of malt extract, 400 g of corn flour, 50 g of soy flour, 110 g of sugar beet syrup, 51 g of agar, 90 g of yeast extract, 31.5 ml of propionic acid, and 7.5 g of Nipagin dissolved in 40 ml of Ethanol, water up to 5 L) in incubators at 25°C prior to the experiment for at least one generation. The incubators maintain 12 h light and dark cycles. For single-cell RNA sequencing (scRNAseq), eye-antennal discs were dissected from late wandering L3 larvae. For single-nuclei RNA sequencing (snRNAseq), eye-antennal discs were dissected from late L3 larvae at 120 h after egg laying. To control for larval density, eggs were deposited on yeast-coated apple agar plates for 1-2 hours and incubated for 24 h before 40 first instar larvae were transferred to food vials for further incubation.

For each dissociation experiment, at least 15 larvae were dissected for no more than 1 h in 400 µl ice-cold 1x PBS. When larval tissue was used for tests, the larvae were everted, and a mix of inner organs (e.g. imaginal discs, gut, brain etc.) was isolated. When eye-antennal discs were used, ~30 eye-antennal discs were dissected (generally from about 15 larvae). All organs were transferred into a microcentrifuge tube containing Storage Buffer (4% BSA, 0.2U Protector RNAse inhibitor (Merck; 3335399001) in PBS). If the sample was to be frozen for later nuclei

extraction, the tube was submerged in liquid nitrogen for 2 min and stored at -80 °C until further processing.

## Recommended dissociation protocol to obtain single-cell suspensions for scRNAseq

In the following, the dissociation protocol is described that was used to obtain the live cells used for scRNAseq. Supplementary Table S1 contains detailed information about the protocol steps that had been varied and tested to achieve efficient dissociation.

~30 eye-antennal discs were dissociated in 10x TrypLE (Thermo Fisher Scientific; A1217701) containing 2.5mg/ml Collagenase (Invitrogen; 17100017) for 30 minutes on the shaker at 30°C and 300 rpm. Every 15 minutes, or, if the digestion time was only 15 min, once after 7.5 min, the discs were pipetted up-and-down 5 times using a 1,000 µl pipet tip to dissociate cell clumps efficiently. The reaction was stopped using Schneider's supplemented medium (SSM, 0.02 mg/ml Insulin in Schneiders Medium (Thermofisher/Gibco; 21720-024)). The suspension was gently pipetted up and down ~17x with a 1,000 µl pipet tip and passed through a 35 µm cell strainer (Corning; 352235). The suspension was centrifuged for 5 min at 1,000 rcf. For low amounts of tissue, the pellet might be small and barely visible on the side wall of the tube. Therefore, it is advantageous to use a swing bucket centrifuge to ensure that the pellet accumulates in the center at the bottom of the tube. The supernatant was removed, and the pellet was resuspended in 1x PBS. The suspension was centrifuged again (see above), the supernatant was removed, and the pellet was resuspended in 0.04% BSA (Invitrogen; 17100017) and 0.2 U/µl Protector RNAse Inhibitor (Sigma-Aldrich; 3335402001) in 1x PBS.

The cells were stained depending on the application: For testing non-fluorescent live-dead assays, 10 µl of a cell suspension were mixed with 10 µl Trypan Blue (Invitrogen; 15250061). 10 µl of this solution were transferred onto a counting chamber and cells were counted using a Zeiss Telaval 31. For fluorescence-based assays, Calcein-AM (green: Sigma-Aldrich; 56496 or violet: Sigma-Aldrich; ThermoFisher Scientific; C34858) was used to stain live cells at a final concentration of 0.5 µg/ml. The suspension was incubated for 30 min to 1 h in the dark at room temperature on a shaker. Either DAPI or Propidium Iodide were used to stain nuclei at a final concentration of 1 µg/ml each and incubated for 10-30 min. The cell suspension was then immediately processed by Fluorescence Activated Cell Sorting (FACS) at the Universitätsmedizin Göttingen or at the Center for Molecular and Cellular Bioengineering Dresden using a Becton Dickinson BD FACSAria™ II Cell Sorter or BD FACSAria™ III Cell

Sorter. In consecutive gating steps, living cells were selected out from debris, damaged cells, and doublets. Events which were positive for Calcein, as well as negative for Propidium Iodide were interpreted as live, undamaged cells. After FACS, cells were visually inspected under the microscope, counted and the volume of the suspension was adjusted with PBS and 0.04% BSA to achieve a concentration of ~1,000 cells per µl to match the optimal requirements for 10X Genomics scRNAseq.

## Recommended dissociation protocol to obtain single nuclei for snRNAseq

Frozen tissue was thawed at 4 °C and kept on ice for the following steps unless specified otherwise. The tissue was transferred into a precooled Dounce homogenizer (2 ml) and 500 µl of Homogenization Buffer (HB) (0.4U/µl RiboLock RNase Inhibitor (ThermoFisher Scientific; EO0381), 0.2U/µl SUPERase In™ RNase Inhibitor (ThermoFisher Scientific; AM2694), 0.10% (v/v) Triton X-100 in NIM2; Nuclei isolation buffer 2 (NIM2): 1 µM DTT, 1x Protease Inhibitor (Promega; G6521) in NIM1; Nuclei isolation buffer 1 (NIM1): 250 mM Sucrose, 25 mM KCl, 5mM $MgCl_2$, 10 mM Tris HCl, ph 8 in nuclease free water) was added. The tissue was homogenized with 8 strokes of the tight pestle and kept on ice whenever possible. If the homogenization seemed incomplete after visual inspection, 1 stroke was added at a time up to a maximum of 11 strokes. The homogenized tissue was filtered through a 30 µm MACS SmartStrainer (Miltenyi; 130-098-458) to exclude larger debris. The homogenizer was furthermore washed with 2x 500 µl of HB to transfer as much of the tissue as possible to the cell strainer. The nuclei suspension was centrifuged at 500 g for 5 min at 4 °C in a swing bucket centrifuge to obtain a nuclei pellet. The supernatant was removed, and the pellet was resuspended in 500 µl Storage Buffer.

For subsequent FACS either 5 µl of a 100 µg/ml DAPI solution (Carl Roth; 6335.1) or 1 drop of NucBlue™ (Hoechst 33342; Invitrogen Live ReadyProbes™; R37605) was added and the nuclei were incubated for 10-20 min for the staining to occur. During the exposure time of the staining, the sample was immediately transferred to FACS (Becton Dickinson (BD™) FACS Aria III Flow Cytometry Cell Sorter) to collect intact nuclei into a 1.5 ml microcentrifuge tube pre-coated with 1% BSA containing 0.04% BSA in 5 µl PBS. The concentration should be ~1,000 nuclei per µl to match the optimal requirements for 10X Genomics snRNAseq. The gates were set to select for DAPI positive nuclei. Particles smaller than 1 µm were excluded to remove small debris and damaged nuclei. Doublets and irregular shaped debris were also filtered out through gating as much as possible. Nozzle size was 100 µm. FACS was performed

at the Universitätsmedizin Göttingen or at the Dresden Concept Genome center using a Becton Dickinson BD FACSAria™ II Cell Sorter or BD FACSAria™ III Cell Sorter. The settings were adjusted using unstained and stained samples.

## Library preparation and 10x Genomics sequencing

scRNAseq and snRNAseq were performed at the Dresden Concept Genome Center on a 10x Genomics Chromium sequencing system. The viability of the sorted cells or quality of nuclei were visually inspected under a light microscope (with 200x magnification) from a small aliquot of cells or nuclei stained with Trypan blue.

Up to 20,000 cells/nuclei were carefully mixed with reverse transcription mix using the Chromium Single Cell 3' Library & Gel beads chemistry v3 (10X Genomics, PN 1000075) and loaded into a Chromium Single Cell B Chip (10X Genomics, PN 1000073) on the 10X Genomics Chromium system [106].

Following the guidelines of the 10X Genomics user manual, the droplets were directly subjected to reverse transcription, the emulsion was broken, and cDNA was purified using Dynabeads MyOne Silane (10X Genomics). After cDNA amplification (11 cycles for cells, 12 cycles for nuclei), the sample was purified and underwent a quality control check on the Fragment Analyzer.

Preparation of single-cell or -nuclei RNA-seq libraries (fragmentation, dA-Tailing, adapter ligation and an indexing PCR step with 12 cycles (cells) or 15 cycles (nuclei)) followed the manufacture's recommendations. After quantification, the libraries were sequenced on an Illumina NextSeq 500 using a high-output flowcell in PE mode (R1: 28 cycles; I1: 8 cycles; R2: 56 cycles) or on the Illumina Novaseq 6000 system with a S2 flowcell in PE mode (R1: 28 cycles; I1: 8 cycles; R2: 94 cycles). An average of 13,000 fragments per cell were sequenced.

## Data analysis

The obtained sequencing data from scRNAseq/snRNAseq were mapped to a genome of the *D. melanogaster* strain Oregon-R (OreR) (FBsn0000276) and reads mapped to individual genes were counted using 10x Genomics Cellranger 5 using default settings for mapping single-cell data. For mapping single-nuclei data, the option --include-introns " was added. The OreR genome was annotated by transferring the annotation of *D. melanogaster* genome r6.37 to a previously sequenced genome of Oregon-R [63, 107] using Liftoff [108].

Further data analyses were performed using R version 4.1.1 (2021-08-10). Specifically, the

package Seurat [109] was used for single-cell specific applications. This includes quality control steps such as calculating the percentage of mitochondrial, ribosomal and heat shock related genes and removing doublets and cells or nuclei of poor quality. Cells of poor quality were defined as expressing more than 3,000 or less than 300 genes. Nuclei of poor quality were defined as the top 1 % of nuclei expressing the highest number of genes or genes in cells, or the top 1 % of nuclei expressing the highest number of genes or less than 300 genes. Genes were kept if they were expressed in at least 5 cells (for scRNAseq) or 3 nuclei (for snRNAseq). Normalization was performed using the SCTransform method [110]. Unbiased clustering was performed in Seurat [111] and marker genes enriched in each cell cluster were identified by differential expression analyses (i.e. genes expressed in a cluster *vs.* all other clusters) followed by a cutoff of log2fold-change > 0.25 and an adjusted p-value < 0.05 (list of cell cluster markers for scRNAseq: Supplementary Table S2; list of cell cluster markers for snRANseq: Supplementary Table S4). Marker genes for each cell cluster were used to test for enrichment of gene ontology (GO) terms (i.e. Biological Process) using the R package gprofiler2 [112, 113] (GO enrichment for scRNAseq: Supplementary Table S3; GO enrichment for snRNAseq: Supplementary Table S5). The top four genes defining each cell cluster were chosen by the lowest adjusted p-value. The ggplot2 package was used to create plots. Note that all scripts and the entire analysis pipeline are available online (https://doi.org/10.25625/YHG4ET).

## Ethics approval and consent to participate

Not applicable

## Consent for publication

Not applicable

## Availability of data and materials

All supplementary tables and figures are part of this submission. All scripts and the entire analysis pipeline are available online (https://doi.org/10.25625/YHG4ET).

## Competing interests

The authors declare that they have no competing interests.

# Funding

This work is supported by a Research Grant of the German Research Foundation (PO 1648/4-1) to NP.

# Author contributions

Conceptualization: GW, NP

Formal analysis: GW

Investigation: GW

Resources: AD, SR

Writing - Original Draft: GW, NP

Writing - Review & Editing: GW, SR, AD, NP

Supervision: NP

Funding acquisition: NP

# Acknowledgments

Many thanks to the CMCB Flow Cytometry Core Facility in Dresden and the Core Facility Cell-Sorting at the UMG in Göttingen for their support with FACS sorting. Thanks to the group of Holger Bastians for providing us with equipment for flow cytometry. We also want to thank Xingbo Xu at the UMG, as well as Ana Veloso at the MDC Berlin for advice on single-nuclei RNA sequencing. Furthermore, we appreciate helpful general input by Anna Schönauer, Jordi Solana and Argyris Papantonis and the critical assessment of the manuscript by Juliana Roscito.

# References

1. Whitfield CW, Cziko A-M, Robinson GE. Gene expression profiles in the brain predict behavior in individual honey bees. Science. 2003;302:296–9. doi:10.1126/science.1086807.
2. Bakken TE, Miller JA, Ding S-L, Sunkin SM, Smith KA, Ng L, et al. A comprehensive transcriptional map of primate brain development. Nature. 2016;535:367–75. doi:10.1038/nature18637.
3. Cardoso-Moreira M, Halbert J, Valloton D, Velten B, Chen C, Shao Y, et al. Gene expression across mammalian organ development. Nature. 2019;571:505–9. doi:10.1038/s41586-019-1338-5.
4. Buchberger E, Reis M, Lu T-H, Posnien N. Cloudy with a Chance of Insights: Context Dependent Gene Regulation and Implications for Evolutionary Studies. Genes (Basel) 2019. doi:10.3390/genes10070492.

5. Shapiro MD, Marks ME, Peichel CL, Blackman BK, Nereng KS, Jónsson B, et al. Genetic and developmental basis of evolutionary pelvic reduction in threespine sticklebacks. Nature. 2004;428:717–23. doi:10.1038/nature02415.
6. McGregor AP, Orgogozo V, Delon I, Zanet J, Srinivasan DG, Payre F, Stern DL. Morphological evolution through multiple cis-regulatory mutations at a single gene. Nature. 2007;448:587–90. doi:10.1038/nature05988.
7. Bendesky A, Kwon Y-M, Lassance J-M, Lewarch CL, Yao S, Peterson BK, et al. The genetic basis of parental care evolution in monogamous mice. Nature. 2017;544:434–9. doi:10.1038/nature22074.
8. Anneser L, Alcantara IC, Gemmer A, Mirkes K, Ryu S, Schuman EM. The neuropeptide Pth2 dynamically senses others via mechanosensation. Nature 2020. doi:10.1038/s41586-020-2988-z.
9. Wang Z, Gerstein M, Snyder M. RNA-Seq: a revolutionary tool for transcriptomics. Nat Rev Genet. 2009;10:57–63. doi:10.1038/nrg2484.
10. Buenrostro JD, Giresi PG, Zaba LC, Chang HY, Greenleaf WJ. Transposition of native chromatin for fast and sensitive epigenomic profiling of open chromatin, DNA-binding proteins and nucleosome position. Nat Meth. 2013;10:1213–8. doi:10.1038/nmeth.2688.
11. Cusanovich DA, Reddington JP, Garfield DA, Daza RM, Aghamirzaie D, Marco-Ferreres R, et al. The cis-regulatory dynamics of embryonic development at single-cell resolution. Nature. 2018;555:538–42. doi:10.1038/nature25981.
12. Kvon EZ, Kazmar T, Stampfel G, Yáñez-Cuna JO, Pagani M, Schernhuber K, et al. Genome-scale functional characterization of Drosophila developmental enhancers in vivo. Nature. 2014;512:91–5. doi:10.1038/nature13395.
13. Kim-Hellmuth S, Aguet F, Oliva M, Muñoz-Aguirre M, Kasela S, Wucher V, et al. Cell type-specific genetic regulation of gene expression across human tissues. Science 2020. doi:10.1126/science.aaz8528.
14. The GTEx Consortium. The GTEx Consortium atlas of genetic regulatory effects across human tissues. Science. 2020;369:1318–30. doi:10.1126/science.aaz1776.
15. Tang F, Barbacioru C, Wang Y, Nordman E, Lee C, Xu N, et al. mRNA-Seq whole-transcriptome analysis of a single cell. Nat Meth. 2009;6:377–82. doi:10.1038/nmeth.1315.
16. Li H, Janssens J, Waegeneer M de, Kolluru SS, Davie K, Gardeux V, et al. Fly Cell Atlas: A single-nucleus transcriptomic atlas of the adult fruit fly. Science. 2022;375:eabk2432. doi:10.1126/science.abk2432.
17. Davie K, Janssens J, Koldere D, Waegeneer M de, Pech U, Kreft Ł, et al. A Single-Cell Transcriptome Atlas of the Aging Drosophila Brain. Cell. 2018;174:982-998.e20. doi:10.1016/j.cell.2018.05.057.
18. Cao J, Packer JS, Ramani V, Cusanovich DA, Huynh C, Daza R, et al. Comprehensive single-cell transcriptional profiling of a multicellular organism. Science. 2017;357:661–7. doi:10.1126/science.aam8940.
19. The Tabula Muris Consortium. A single-cell transcriptomic atlas characterizes ageing tissues in the mouse. Nature. 2020;583:590–5. doi:10.1038/s41586-020-2496-1.
20. Özel MN, Simon F, Jafari S, Holguera I, Chen Y-C, Benhra N, et al. Neuronal diversity and convergence in a visual system developmental atlas. Nature. 2021;589:88–95. doi:10.1038/s41586-020-2879-3.
21. Kumar MP, Du J, Lagoudas G, Jiao Y, Sawyer A, Drummond DC, et al. Analysis of Single-Cell RNA-Seq Identifies Cell-Cell Communication Associated with Tumor Characteristics. Cell Rep. 2018;25:1458-1468.e4. doi:10.1016/j.celrep.2018.10.047.

22. Stubbington MJT, Rozenblatt-Rosen O, Regev A, Teichmann SA. Single-cell transcriptomics to explore the immune system in health and disease. Science. 2017;358:58–63. doi:10.1126/science.aan6828.
23. Shalek AK, Satija R, Adiconis X, Gertner RS, Gaublomme JT, Raychowdhury R, et al. Single-cell transcriptomics reveals bimodality in expression and splicing in immune cells. Nature. 2013;498:236–40. doi:10.1038/nature12172.
24. Musser JM, Schippers KJ, Nickel M, Mizzon G, Kohn AB, Pape C, et al. Profiling cellular diversity in sponges informs animal cell type and nervous system evolution. Science. 2021;374:717–23. doi:10.1126/science.abj2949.
25. Sebé-Pedrós A, Saudemont B, Chomsky E, Plessier F, Mailhé M-P, Renno J, et al. Cnidarian Cell Type Diversity and Regulation Revealed by Whole-Organism Single-Cell RNA-Seq. Cell. 2018;173:1520-1534.e20. doi:10.1016/j.cell.2018.05.019.
26. Klimovich A, Giacomello S, Björklund Å, Faure L, Kaucka M, Giez C, et al. Prototypical pacemaker neurons interact with the resident microbiota. Proc Natl Acad Sci U S A. 2020;117:17854–63. doi:10.1073/pnas.1920469117.
27. Chari T, Weissbourd B, Gehring J, Ferraioli A, Leclère L, Herl M, et al. Whole-animal multiplexed single-cell RNA-seq reveals transcriptional shifts across Clytia medusa cell types. Sci Adv. 2021;7:eabh1683. doi:10.1126/sciadv.abh1683.
28. Vergara HM, Bertucci PY, Hantz P, Tosches MA, Achim K, Vopalensky P, Arendt D. Whole-organism cellular gene-expression atlas reveals conserved cell types in the ventral nerve cord of Platynereis dumerilii. Proc Natl Acad Sci U S A. 2017;114:5878–85. doi:10.1073/pnas.1610602114.
29. Plass M, Solana J, Wolf FA, Ayoub S, Misios A, Glažar P, et al. Cell type atlas and lineage tree of a whole complex animal by single-cell transcriptomics. Science 2018. doi:10.1126/science.aaq1723.
30. Fincher CT, Wurtzel O, Hoog T de, Kravarik KM, Reddien PW. Cell type transcriptome atlas for the planarian Schmidtea mediterranea. Science 2018. doi:10.1126/science.aaq1736.
31. Sheng L, Shields EJ, Gospocic J, Glastad KM, Ratchasanmuang P, Berger SL, et al. Social reprogramming in ants induces longevity-associated glia remodeling. Sci Adv. 2020;6:eaba9869. doi:10.1126/sciadv.aba9869.
32. Tosches MA, Yamawaki TM, Naumann RK, Jacobi AA, Tushev G, Laurent G. Evolution of pallium, hippocampus, and cortical cell types revealed by single-cell transcriptomics in reptiles. Science. 2018;360:881–8. doi:10.1126/science.aar4237.
33. Chen D, Sun J, Zhu J, Ding X, Lan T, Wang X, et al. Single cell atlas for 11 non-model mammals, reptiles and birds. Nat Commun. 2021;12:7083. doi:10.1038/s41467-021-27162-2.
34. Bakken TE, Jorstad NL, Hu Q, Lake BB, Tian W, Kalmbach BE, et al. Comparative cellular analysis of motor cortex in human, marmoset and mouse. Nature. 2021;598:111–9. doi:10.1038/s41586-021-03465-8.
35. Liu T, Li J, Yu L, Sun H-X, Li J, Dong G, et al. Cross-species single-cell transcriptomic analysis reveals pre-gastrulation developmental differences among pigs, monkeys, and humans. Cell Discov. 2021;7:8. doi:10.1038/s41421-020-00238-x.
36. Kolodziejczyk AA, Kim JK, Svensson V, Marioni JC, Teichmann SA. The technology and biology of single-cell RNA sequencing. Molecular Cell. 2015;58:610–20. doi:10.1016/j.molcel.2015.04.005.
37. Wu AR, Wang J, Streets AM, Huang Y. Single-Cell Transcriptional Analysis. Annu Rev Anal Chem (Palo Alto Calif). 2017;10:439–62. doi:10.1146/annurev-anchem-061516-045228.

38. Islam S, Kjällquist U, Moliner A, Zajac P, Fan J-B, Lönnerberg P, Linnarsson S. Characterization of the single-cell transcriptional landscape by highly multiplex RNA-seq. Genome Research. 2011;21:1160–7. doi:10.1101/gr.110882.110.
39. Macosko EZ, Basu A, Satija R, Nemesh J, Shekhar K, Goldman M, et al. Highly Parallel Genome-wide Expression Profiling of Individual Cells Using Nanoliter Droplets. Cell. 2015;161:1202–14. doi:10.1016/j.cell.2015.05.002.
40. Svensson V, Vento-Tormo R, Teichmann SA. Exponential scaling of single-cell RNA-seq in the past decade. Nature Protocols. 2018;13:599–604. doi:10.1038/nprot.2017.149.
41. Khan SJ, Abidi SNF, Tian Y, Skinner A, Smith-Bolton RK. A rapid, gentle and scalable method for dissociation and fluorescent sorting of imaginal disc cells for mRNA sequencing. Fly (Austin). 2016;10:73–80. doi:10.1080/19336934.2016.1173296.
42. Hodges GM, Livingston DC, Franks LM. The localization of trypsin in cultured mammalian cells. J Cell Sci. 1973;12:887–902. doi:10.1242/jcs.12.3.887.
43. Snow C, Allen A. The release of radioactive nucleic acids and mucoproteins by trypsin and ethylenediaminetetra-acetate treatment of baby-hamster cells in tissue culture. Biochem J. 1970;119:707–14. doi:10.1042/bj1190707.
44. Huang H-L, Hsing H-W, Lai T-C, Chen Y-W, Lee T-R, Chan H-T, et al. Trypsin-induced proteome alteration during cell subculture in mammalian cells. J Biomed Sci. 2010;17:36. doi:10.1186/1423-0127-17-36.
45. Vrtačnik P, Kos Š, Bustin SA, Marc J, Ostanek B. Influence of trypsinization and alternative procedures for cell preparation before RNA extraction on RNA integrity. Anal Biochem. 2014;463:38–44. doi:10.1016/j.ab.2014.06.017.
46. Gehring W, Noethiger R. The imaginal discs of Drosophila. In: Waddington, C.H., Counce-Nicklas, S., editor. Developmental Systems: Insects: London-New York: Academic Press; 1973.
47. Garcia-Bellido A, Merriam JR. Cell lineage of the imaginal discs in Drosophila gynandromorphs. J. Exp. Zool. 1969;170:61–75. doi:10.1002/jez.1401700106.
48. Becker HJ. Ueber Roentgenmosaikflecken Und Defektmutationen Am Auge Von Drosophila Und Die Entwicklungsphysiologie Des Auges. Zeitschrift für Induktive Abstammungs- und Vererbungslehre. 1957;88:333–73. doi:10.1007/bf00309128.
49. Cohen SM. Imaginal Disc Development. In: Bate M, Martinez Arias A, editors. The development of Drosophila melanogaster. Cold Spring Harbor: Cold Spring Harbor Laboratory Press; 1993.
50. Domínguez M, Casares F. Organ specification-growth control connection: new in-sights from the Drosophila eye-antennal disc. Dev Dyn. 2005;232:673–84. doi:10.1002/dvdy.20311.
51. Kumar JP. The fly eye: Through the looking glass. Dev Dyn. 2018;247:111–23. doi:10.1002/dvdy.24585.
52. Morata G, Lawrence PA. Development of the eye-antenna imaginal disc of Drosophila. Developmental Biology. 1979;70:355–71. doi:10.1016/0012-1606(79)90033-2.
53. Haynie JL, Bryant PJ. Development of the eye-antenna imaginal disc and morphogenesis of the adult head in Drosophila melanogaster. J. Exp. Zool. 1986;237:293–308. doi:10.1002/jez.1402370302.
54. Keesey IW, Grabe V, Gruber L, Koerte S, Obiero GF, Bolton G, et al. Inverse resource allocation between vision and olfaction across the genus Drosophila. Nat Commun. 2019;10:1162. doi:10.1038/s41467-019-09087-z.
55. Posnien N, Hopfen C, Hilbrant M, Ramos-Womack M, Murat S, Schönauer A, et al. Evolution of eye morphology and rhodopsin expression in the Drosophila melanogaster species subgroup. PLoS One. 2012;7:e37346. doi:10.1371/journal.pone.0037346.

56. Hämmerle B, Ferrús A. Expression of enhancers is altered in Drosophila melanogaster hybrids. Evol Dev. 2003;5:221–30. doi:10.1046/j.1525-142x.2003.03030.x.
57. Norry FM, Gomez FH. Quantitative Trait Loci and Antagonistic Associations for Two Developmentally Related Traits in the Drosophila Head. J Insect Sci 2017. doi:10.1093/jisesa/iew115.
58. Gaspar P, Arif S, Sumner-Rooney L, Kittelmann M, Bodey AJ, Stern DL, et al. Characterization of the Genetic Architecture Underlying Eye Size Variation Within Drosophila melanogaster and Drosophila simulans. G3 (Bethesda). 2020;10:1005–18. doi:10.1534/g3.119.400877.
59. Ramaekers A, Claeys A, Kapun M, Mouchel-Vielh E, Potier D, Weinberger S, et al. Altering the Temporal Regulation of One Transcription Factor Drives Evolutionary Trade-Offs between Head Sensory Organs. Dev Cell. 2019;50:780-792.e7. doi:10.1016/j.devcel.2019.07.027.
60. Reis M, Wiegleb G, Claude J, Lata R, Horchler B, Ha N-T, et al. Multiple loci linked to inversions are associated with eye size variation in species of the Drosophila virilis phylad. Sci Rep. 2020;10:12832. doi:10.1038/s41598-020-69719-z.
61. Norry FM, Vilardi JC, Hasson E. Negative genetic correlation between traits of the Drosophila head, and interspecific divergence in head shape. Heredity (Edinb). 2000;85 (Pt 2):177–83. doi:10.1046/j.1365-2540.2000.00735.x.
62. Casares F, McGregor AP. The evolution and development of eye size in flies. Wiley Interdiscip Rev Dev Biol. 2021;10:e380. doi:10.1002/wdev.380.
63. Buchberger E, Bilen A, Ayaz S, Salamanca D, Matas de Las Heras C, Niksic A, et al. Variation in Pleiotropic Hub Gene Expression Is Associated with Interspecific Differences in Head Shape and Eye Size in Drosophila. Mol Biol Evol. 2021;38:1924–42. doi:10.1093/molbev/msaa335.
64. Arif S, Hilbrant M, Hopfen C, Almudi I, Nunes MDS, Posnien N, et al. Genetic and developmental analysis of differences in eye and face morphology between Drosophila simulans and Drosophila mauritiana. Evol Dev. 2013;15:257–67. doi:10.1111/ede.12027.
65. Ariss MM, Islam ABMMK, Critcher M, Zappia MP, Frolov MV. Single cell RNA-sequencing identifies a metabolic aspect of apoptosis in Rbf mutant. Nat Commun. 2018;9:5024. doi:10.1038/s41467-018-07540-z.
66. Bravo González-Blas C, Quan X-J, Duran-Romaña R, Taskiran II, Koldere D, Davie K, et al. Identification of genomic enhancers through spatial integration of single-cell transcriptomics and epigenomics. Mol Syst Biol. 2020;16:e9438. doi:10.15252/msb.20209438.
67. Pappenheimer AM. EXPERIMENTAL STUDIES UPON LYMPHOCYTES : I. THE REACTIONS OF LYMPHOCYTES UNDER VARIOUS EXPERIMENTAL CONDITIONS. J Exp Med. 1917;25:633–50. doi:10.1084/jem.25.5.633.
68. Chan LL-Y, Kuksin D, Laverty DJ, Saldi S, Qiu J. Morphological observation and analysis using automated image cytometry for the comparison of trypan blue and fluorescence-based viability detection method. Cytotechnology. 2015;67:461–73. doi:10.1007/s10616-014-9704-5.
69. Rabani M, Levin JZ, Fan L, Adiconis X, Raychowdhury R, Garber M, et al. Metabolic labeling of RNA uncovers principles of RNA production and degradation dynamics in mammalian cells. Nat Biotechnol. 2011;29:436–42. doi:10.1038/nbt.1861.
70. Rabani M, Raychowdhury R, Jovanovic M, Rooney M, Stumpo DJ, Pauli A, et al. High-resolution sequencing and modeling identifies distinct dynamic RNA regulatory strategies. Cell. 2014;159:1698–710. doi:10.1016/j.cell.2014.11.015.

71. Dong PDS, Dicks JS, Panganiban G. Distal-less and homothorax regulate multiple targets to pattern the Drosophila antenna. Development. 2002;129:1967–74. doi:10.1242/dev.129.8.1967.
72. Blochlinger K, Jan LY, Jan YN. Postembryonic patterns of expression of cut, a locus regulating sensory organ identity in Drosophila. Development. 1993;117:441–50. doi:10.1242/dev.117.2.441.
73. Czerny T, Halder G, Kloter U, Souabni A, Gehring WJ, Busslinger M. twin of eyeless, a Second Pax-6 Gene of Drosophila, Acts Upstream of eyeless in the Control of Eye Development. Molecular Cell. 1999;3:297–307. doi:10.1016/s1097-2765(00)80457-8.
74. Royet J, Finkelstein R. Pattern formation in Drosophila head development: the role of the orthodenticle homeobox gene. Development. 1995;121:3561–72. doi:10.1242/dev.121.11.3561.
75. Pichaud F, Casares F. homothorax and iroquois-C genes are required for the establishment of territories within the developing eye disc. Mechanisms of Development. 2000;96:15–25. doi:10.1016/S0925-4773(00)00372-5.
76. Pai CY, Kuo TS, Jaw TJ, Kurant E, Chen CT, Bessarab DA, et al. The Homothorax homeoprotein activates the nuclear localization of another homeoprotein, extradenticle, and suppresses eye development in Drosophila. Genes Dev. 1998;12:435–46. doi:10.1101/gad.12.3.435.
77. Wurmbach E, Wech I, Preiss A. The Enhancer of split complex of Drosophila melanogaster harbors three classes of Notch responsive genes. Mechanisms of Development. 1999;80:171–80. doi:10.1016/S0925-4773(98)00212-3.
78. Wolff T, READY DF. Pattern formation in the Drosophila retina. In: Bate M, Martinez-Arias a, editors. The development of Drosophila melanogaster. II. Cold Spring Harbor: Cold Spring Harbor Laboratory Press; 1993. p. 1277–1325.
79. Martin PF. Direct determination of the growth rate of Drosophila imaginal discs. J. Exp. Zool. 1982;222:97–102. doi:10.1002/jez.1402220113.
80. Wu H, Kirita Y, Donnelly EL, Humphreys BD. Advantages of Single-Nucleus over Single-Cell RNA Sequencing of Adult Kidney: Rare Cell Types and Novel Cell States Revealed in Fibrosis. J Am Soc Nephrol. 2019;30:23–32. doi:10.1681/ASN.2018090912.
81. Yim AKY, Wang PL, Bermingham JR, Hackett A, Strickland A, Miller TM, et al. Disentangling glial diversity in peripheral nerves at single-nuclei resolution. Nat Neurosci. 2022;25:238–51. doi:10.1038/s41593-021-01005-1.
82. Lake BB, Codeluppi S, Yung YC, Gao D, Chun J, Kharchenko PV, et al. A comparative strategy for single-nucleus and single-cell transcriptomes confirms accuracy in predicted cell-type expression from nuclear RNA. Sci Rep. 2017;7:6031. doi:10.1038/s41598-017-04426-w.
83. Grindberg RV, Yee-Greenbaum JL, McConnell MJ, Novotny M, O'Shaughnessy AL, Lambert GM, et al. RNA-sequencing from single nuclei. Proc Natl Acad Sci U S A. 2013;110:19802–7. doi:10.1073/pnas.1319700110.
84. 10X Genomics. Nuclei Isolation from Cell Suspensions & Tissues for Single Cell RNA Sequencing: CG000124 • Rev F. 2021. https://assets.ctfassets.net/an68im79xiti/2HNFgXau0ntv1BhS4ffn6n/71a29daf18e5f7c30cf06b5b4f829e44/CG000124_Demonstrated_Protocol_Nuclei_isolation_RevF.pdf. Accessed 28 Apr 2022.
85. Litvinukova M, Lindberg E, Maatz H, Zhang H, Radke M, Gotthardt M, et al. Single Cell and Single Nuclei Analysis Human Heart Tissue. protocols.io 2018. doi:10.17504/protocols.io.veae3ae.

86. Tosti L, Hang Y, Debnath O, Tiesmeyer S, Trefzer T, Steiger K, et al. Single-Nucleus and In Situ RNA-Sequencing Reveal Cell Topographies in the Human Pancreas. Gastroenterology. 2021;160:1330-1344.e11. doi:10.1053/j.gastro.2020.11.010.
87. Butler SJ, Ray S, Hiromi Y. klingon, a novel member of the Drosophila immunoglobulin superfamily, is required for the development of the R7 photoreceptor neuron. Development. 1997;124:781–92. doi:10.1242/dev.124.4.781.
88. St Pierre SE, Galindo MI, Couso JP, Thor S. Control of Drosophila imaginal disc development by rotund and roughened eye: differentially expressed transcripts of the same gene encoding functionally distinct zinc finger proteins. Development. 2002;129:1273–81. doi:10.1242/dev.129.5.1273.
89. Lake BB, Chen S, Sos BC, Fan J, Kaeser GE, Yung YC, et al. Integrative single-cell analysis of transcriptional and epigenetic states in the human adult brain. Nat Biotechnol. 2018;36:70–80. doi:10.1038/nbt.4038.
90. Bakken TE, Hodge RD, Miller JA, Yao Z, Nguyen TN, Aevermann B, et al. Single-nucleus and single-cell transcriptomes compared in matched cortical cell types. PLoS One. 2018;13:e0209648. doi:10.1371/journal.pone.0209648.
91. Estella C, Mann RS. Non-redundant selector and growth-promoting functions of two sister genes, buttonhead and Sp1, in Drosophila leg development. PLoS Genet. 2010;6:e1001001. doi:10.1371/journal.pgen.1001001.
92. Grubbs N, Leach M, Su X, Petrisko T, Rosario JB, Mahaffey JW. New components of Drosophila leg development identified through genome wide association studies. PLoS One. 2013;8:e60261. doi:10.1371/journal.pone.0060261.
93. Mao Y, Freeman M. Fasciclin 2, the Drosophila orthologue of neural cell-adhesion molecule, inhibits EGF receptor signalling. Development. 2009;136:473–81. doi:10.1242/dev.026054.
94. Choi K-W, Benzer S. Rotation of photoreceptor clusters in the developing drosophila eye requires the nemo gene. Cell. 1994;78:125–36. doi:10.1016/0092-8674(94)90579-7.
95. Kim SY, Renihan MK, Boulianne GL. Characterization of big bang, a novel gene encoding for PDZ domain-containing proteins that are dynamically expressed throughout Drosophila development. Gene Expr Patterns. 2006;6:504–18. doi:10.1016/j.modgep.2005.10.009.
96. Krishnaswami SR, Grindberg RV, Novotny M, Venepally P, Lacar B, Bhutani K, et al. Using single nuclei for RNA-seq to capture the transcriptome of postmortem neurons. Nature Protocols. 2016;11:499–524. doi:10.1038/nprot.2016.015.
97. Habib N, Li Y, Heidenreich M, Swiech L, Avraham-Davidi I, Trombetta JJ, et al. Div-Seq: Single-nucleus RNA-Seq reveals dynamics of rare adult newborn neurons. Science. 2016;353:925–8. doi:10.1126/science.aad7038.
98. Ding J, Adiconis X, Simmons SK, Kowalczyk MS, Hession CC, Marjanovic ND, et al. Systematic comparison of single-cell and single-nucleus RNA-sequencing methods. Nat Biotechnol. 2020;38:737–46. doi:10.1038/s41587-020-0465-8.
99. Slyper M, Porter CBM, Ashenberg O, Waldman J, Drokhlyansky E, Wakiro I, et al. A single-cell and single-nucleus RNA-Seq toolbox for fresh and frozen human tumors. Nat Med. 2020;26:792–802. doi:10.1038/s41591-020-0844-1.
100. Darmanis S, Sloan SA, Zhang Y, Enge M, Caneda C, Shuer LM, et al. A survey of human brain transcriptome diversity at the single cell level. Proc Natl Acad Sci U S A. 2015;112:7285–90. doi:10.1073/pnas.1507125112.
101. Palazzo AF, Lee ES. Sequence Determinants for Nuclear Retention and Cytoplasmic Export of mRNAs and lncRNAs. Front Genet. 2018;9:440. doi:10.3389/fgene.2018.00440.

102. Wickramasinghe VO, Laskey RA. Control of mammalian gene expression by selective mRNA export. Nat Rev Mol Cell Biol. 2015;16:431–42. doi:10.1038/nrm4010.
103. Gehring NH, Roignant J-Y. Anything but Ordinary - Emerging Splicing Mechanisms in Eukaryotic Gene Regulation. Trends Genet. 2021;37:355–72. doi:10.1016/j.tig.2020.10.008.
104. Galloway A, Cowling VH. mRNA cap regulation in mammalian cell function and fate. Biochim Biophys Acta Gene Regul Mech. 2019;1862:270–9. doi:10.1016/j.bbagrm.2018.09.011.
105. Mittleman BE, Pott S, Warland S, Zeng T, Mu Z, Kaur M, et al. Alternative polyadenylation mediates genetic regulation of gene expression. Elife 2020. doi:10.7554/eLife.57492.
106. Zheng GXY, Terry JM, Belgrader P, Ryvkin P, Bent ZW, Wilson R, et al. Massively parallel digital transcriptional profiling of single cells. Nat Commun. 2017;8:14049. doi:10.1038/ncomms14049.
107. Torres-Oliva M, Almudi I, McGregor AP, Posnien N. A robust (re-)annotation approach to generate unbiased mapping references for RNA-seq-based analyses of differential expression across closely related species. BMC Genomics. 2016;17:392. doi:10.1186/s12864-016-2646-x.
108. Shumate A, Salzberg SL. Liftoff: accurate mapping of gene annotations. Bioinformatics 2020. doi:10.1093/bioinformatics/btaa1016.
109. Hao Y, Hao S, Andersen-Nissen E, Mauck WM, Zheng S, Butler A, et al. Integrated analysis of multimodal single-cell data. Cell. 2021;184:3573-3587.e29. doi:10.1016/j.cell.2021.04.048.
110. Hafemeister C, Satija R. Normalization and variance stabilization of single-cell RNA-seq data using regularized negative binomial regression. Genome Biol. 2019;20:296. doi:10.1186/s13059-019-1874-1.
111. Waltman L, van Eck NJ. A smart local moving algorithm for large-scale modularity-based community detection. Eur. Phys. J. B 2013. doi:10.1140/epjb/e2013-40829-0.
112. Raudvere U, Kolberg L, Kuzmin I, Arak T, Adler P, Peterson H, Vilo J. g:Profiler: a web server for functional enrichment analysis and conversions of gene lists (2019 update). Nucleic Acids Res. 2019;47:W191-W198. doi:10.1093/nar/gkz369.
113. Kolberg L, Raudvere U, Kuzmin I, Vilo J, Peterson H. gprofiler2 -- an R package for gene list functional enrichment analysis and namespace conversion toolset g:Profiler. F1000Res 2020. doi:10.12688/f1000research.24956.2.

# Figure Legends

**Figure 1. Evaluation of read distribution after scRNAseq and snRNAseq.**
**(A)** Total amount of genes (features) over percentage of mitochondrial reads, per cell each. The dashed line indicates a threshold of 10% of reads attributed to mitochondrial genes. In single-cell RNA sequencing data, approximately 14% of cells show a high (>10%) proportion of mitochondrial gene reads on the total number of reads. | **(B)** Total amount of genes (features) over Percentage of mitochondrial reads, per cell each in single-nuclei RNA sequencing data. The dashed line indicates a threshold of 10% of reads attributed to mitochondrial genes. In most nuclei, only a low percentage of reads is attributed to mitochondrial genes. | **(C)** Number of reads found in nuclei (y-axis) over the number of reads of those same genes found in cells.

878 The basis are normalized datasets. Ribosomal genes are highlighted in blue and heat shock
879 genes in red. Ribosomal genes are defined as genes starting RpS- or RpL-. Heat shock genes
880 are defined as genes encoding heat shock proteins, starting Hsp-.
881
882 **Figure 2. Most variable genes and marker genes for cell clusters after scRNAseq and**
883 **snRNAseq.**
884 **(A)** Variable feature plot of scRNAseq data of dissociated cells. The top 10 variable genes are
885 labeled. These genes are the ones having the strongest influence on clustering and cell type
886 identification. **(B)** Dot plot of the top 4 marker genes (X-axis) for each cell cluster (Y-axis)
887 obtained after scRNAseq. The size of the dots represents the percentage of cells expressing
888 each gene. The color intensity represents the average expression level. **(C)** Variable feature
889 plot of snRNAseq data of isolated nuclei. The top 10 variable genes are labeled. These genes
890 are the ones having the strongest influence on clustering and cell type identification. **(D)** Dot
891 plot of the top 4 marker genes (X-axis) for each cell cluster (Y-axis) obtained after snRNAseq.
892 The size of the dots represents the percentage of cells expressing each gene. The color intensity
893 represents the average expression level.
894

# Supplementary Files

This is a list of supplementary files associated with this preprint. Click to download.

- SupplementaryTable2clustermarkergenescells.xlsx
- WieglebetalSuppl.pdf
- SupplementaryTable3GOBPcells.xlsx
- SupplementaryTable4clustermarkergenesnuclei.xlsx
- SupplementaryTable5GOBPnuclei.xlsx